Research Article

Visible Light Photoelectrochemical Properties of N-Doped TiO₂ Nanorod Arrays from TiN

Zheng Xie,[1,2] **Yongbin Zhang,**[3] **Xiangxuan Liu,**[2] **Weipeng Wang,**[1] **Peng Zhan,**[1] **Zhengcao Li,**[1] **and Zhengjun Zhang**[1]

[1] *The State Key Laboratory for New Ceramics and Fine Processing, School of Materials Science and Engineering, Tsinghua University, Beijing 100084, China*
[2] *High-Tech Institute of Xi'an, Shaanxi 710025, China*
[3] *Science and Technology on Surface Physics and Chemistry Laboratory, Mianyang 621907, China*

Correspondence should be addressed to Zhengjun Zhang; zjzhang@tsinghua.edu.cn

N-doped TiO₂ nanorod arrays (NRAs) were prepared by annealing the TiN nanorod arrays (NRAs) which were deposited by using oblique angle deposition (OAD) technique. The TiN NRAs were annealed at 330°C for different times (5, 15, 30, 60, and 120 min). The band gaps of annealed TiN NRAs (i.e., N-doped TiO₂ NRAs) show a significant variance with annealing time, and can be controlled readily by varying annealing time. All of the N-doped TiO₂ NRAs exhibit an enhancement in photocurrent intensity in visible light compared with that of pure TiO₂ and TiN, and the one annealed for 15 min shows the maximum photocurrent intensity owning to the optimal N dopant concentration. The results show that the N-doped TiO₂ NRAs, of which the band gap can be tuned easily, are a very promising material for application in photocatalysis.

1. Introduction

Since the first report of photocatalytic splitting of water using titanium dioxide (TiO₂) photoanode by Fujishima and Honda in 1972 [1], TiO₂ has been extensively studied and has been considered as one of the superior candidates for solving environmental concerns due to its cheapness, photostability, chemical inertness, nontoxicity, and strong photocatalytic activity [2]. However, the wide applications of TiO₂ are limited due to its large band gap (*ca*. 3.2 eV and 3.0 eV for anatase and rutile, resp.), which makes it active only under ultraviolet (UV) (i.e., using less than *ca*. 5% of the solar energy) [3]. To enhance the solar energy conversion efficiency of TiO₂, one of the strategies is to enhance its photoresponse activity in the visible light, which composes a greater portion (*ca*. 45%) of the solar spectrum [4]. Visible light activity of the TiO₂ has been achieved by several strategies such as coupling with dyes [5] and sensitizing with semiconductors [6] which have proper conduction band levels and doping with impurities [7]. Doping with nonmetal ion may be

a promising way to avoid the deterioration of the thermal stability of TiO₂ lattice [8]. Many reported doping with various substances, such as with nitrogen [9], sulfur [10], fluoride [11], and carbon [12]. Since Asahi et al. [9] reported that the band gap narrowed by N doping improved the photocatalytic activity of TiO₂ in visible light, N doping has been considered as one of the most effective approaches to shift the optical response of TiO₂ from the UV to the visible spectral range. There are mainly two major ways to prepare the N-doped TiO₂. One of which is based on incorporation of N into TiO₂ lattice by ion-implantation technique [13], reactive magnetron sputtering [14], hydrothermal method [15], and so forth. The other method, also used in this work, relies on oxidation of TiN$_x$, [16, 17] which is a facile method to fabricate N-doped TiO₂.

The other way to enhance the solar conversion efficiency is to obtain good electron-hole separation characteristics by reducing the recombination centers and increasing the charge transfer [18]. Fabricating nanostructures such as nanoparticles, nanotubes, nanowires, nanobelts, and nanorods is

a promising way to enhance solar energy conversion efficiency of TiO_2, since nanostructures exhibit many desirable characteristics for effective photocatalysis such as efficient and tunable optical absorption, large surface areas, short charge carrier diffusion lengths, and low reflectivity [19]. One-dimensional (1D) nanostructures are expected to have improved charge-transport properties compared to zero-dimensional (0D) nanostructures because of the direct conduction pathways in nanorods versus electron hopping in nanoparticles system. 1D nanostructures can be obtained by organometallic chemical vapor deposition (OMCVD) [20], hydrothermal processes [21], glancing angle deposition (GLAD) [22], and oblique angle deposition (OAD) [23]. Compared with other fabrication methods, OAD technique provides a simple way to produce large area, uniformed, aligned nanorod arrays with controlled porosity. OAD technique is a unique physical vapor deposition process, where the vapor flux is incident onto a substrate at a large angle θ ($\theta > 70°$) with respect to the substrate normal. Due to the self-shadowing effect, well aligned and separated nanorod arrays, tilting toward the direction of the vapor flux, can be produced [24]. The film prepared by OAD technique presents a porous microstructure, where nanometer size columns with a high internal porosity are separated by wide pores which extend from the substrate to the film surface [25]. This microstructure is of significant advantage in increasing the interface of nanorod and solution. Moreover, films deposited on glass, FTO, Si, or other substrates by OAD technique are convenient to be reused compared with the 0D nanostructures.

Herein, we report the visible light photoelectrochemical properties of N-doped TiO_2 nanorod arrays (NRAs) by oxidation of TiN nanorod arrays (NRAs), which are fabricated using OAD technique. The concentration of N dopant in the TiO_2 is controlled by changing the annealing time at 330°C. The photoelectrochemical properties of the N-doped TiO_2 NRAs in visible light are improved obviously compared with that of bare TiO_2 NRAs and TiN NRAs.

2. Experimental Details

2.1. Fabrication of N-Doped TiO_2 NRAs. The TiN NRAs were deposited on quartz and F-doped SnO_2 (FTO) substrates by using oblique angle deposition technique (OAD) described elsewhere [26], of which quartz substrates were used for UV-vis transmittance measurement. The substrates were ultrasonically cleaned sequentially in acetone and alcohol and then rinsed in deionized water for 5 minutes each. The system was pumped down to a vacuum level of 2×10^{-5} Pa, and then TiN NRAs were deposited at a deposition rate of $0.5 \, nm \, s^{-1}$, of which the thickness was monitored by a quartz crystal microbalance. To produce aligned TiN NRAs, the incident beam of TiN flux was set at *ca.* 85° from the normal of the substrate, and the substrate temperature was controlled at *ca.* −20°C using liquid nitrogen for maintaining the temperature. The N-doped TiO_2 NRAs were obtained by oxidizing the as-prepared TiN NRAs in a tube furnace under atmosphere at 330°C, and the N contents in TiO_2 NRAs were controlled by varying the annealing time (i.e., 5 min, 15 min, 30 min,
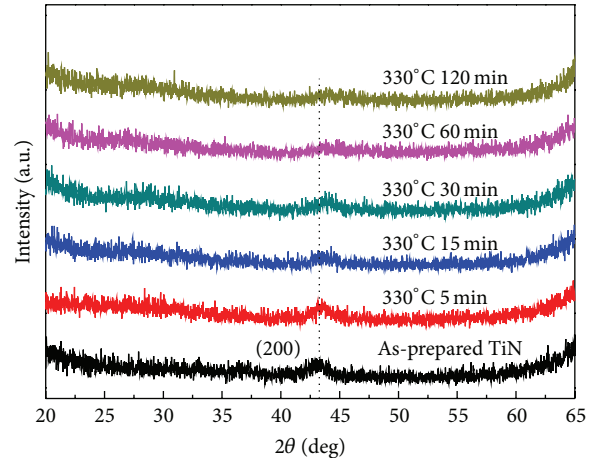

FIGURE 1: XRD patterns of the as-deposited TiN NRAs and the N-doped TiO_2 NRAs annealed at 330°C in atmosphere for different time.

60 min, and 120 min). For the sake of convenience one marks the TiN NRAs annealed for 5 min, 15 min, 30 min, 60 min, and 120 min as 5 N-TiO_2, 15 N-TiO_2, 30 N-TiO_2, 60 N-TiO_2, and 120 N-TiO_2, respectively.

2.2. Characterizations. The crystal structure of the TiN NRAs and N-doped TiO_2 (annealed TiN NRAs) was characterized by X-ray diffraction (XRD Rigaku 2500) using Cu Kα radiation. The morphology was characterized by using a field emission scanning electron microscopy (SEM JEOL-7001 F). The microstructures of prepared samples were also characterized with a transmission electron microscope (TEM JEOL-2010 F). Transmittance spectra were recorded using a UV-vis spectrophotometer (PerkinElmer Lambda 35). The XPS experiments were performed on the samples with PHI 5300 (Perkin Elmer). The binding energy of the XPS spectra was calibrated with the reference to the C $1s$ peak at 284.6 eV.

Photoelectrochemical measurements were performed in a 250 mL quartz cell using a three-electrode configuration, which are composed of the prepared samples as a working electrode, a Pt foil as a counter electrode, a saturated Ag/AgCl as a reference electrode, and 1 M KOH as an electrolyte. The photocurrent intensity versus potential (*I-V* curve) measurements was performed by an electrochemistry workstation (CHI 660, Chenhua Instrument). The working electrode was illuminated with a 300 W Xe lamp. An ultraviolet cutoff filter was inserted between the light source and the quartz cell to exclude UV light with the wavelength below 420 nm. The photocurrent dynamics of the working electrode were recorded according to the response to sudden switching on and off at 0 V bias versus Ag/AgCl.

3. Results and Discussion

Figure 1 displays the XRD patterns of the as-deposited TiN NRAs and the TiN NRAs annealed in air at 330°C for different times. It can be seen that the as-deposited TiN NRAs exhibit structure with (200) orientations (JCPDS 38-1420). The TiN
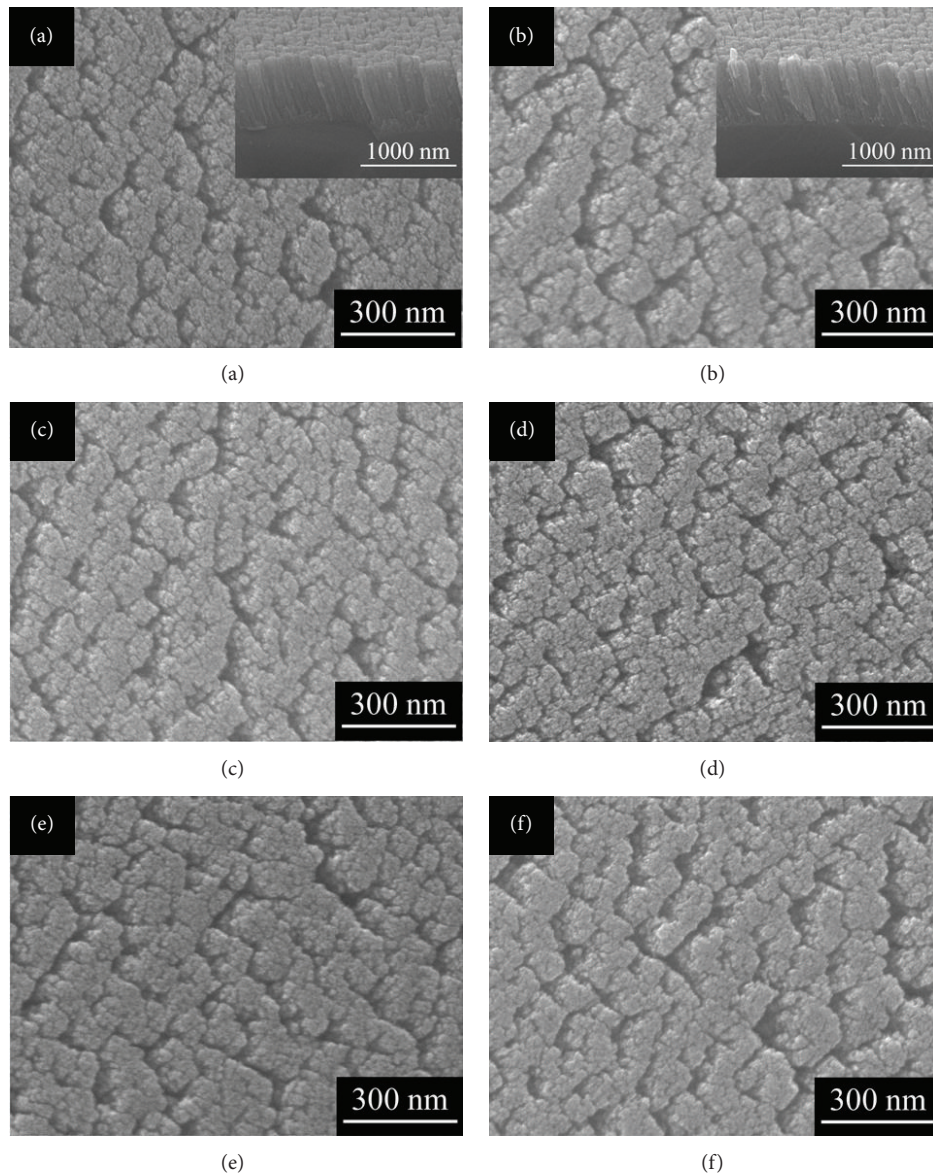
FIGURE 2: SEM images of the as-deposited TiN NRAs (a), 5 N-TiO$_2$ NRAs (b), 15 N-TiO$_2$ NRAs (c), 30 N-TiO$_2$ NRAs (d), 60 N-TiO$_2$ NRAs (e), and 120 N-TiO$_2$ NRAs (f). The insets in (a) and (b) are the corresponding SEM images with a tilt angle of 45°.

(200) peak exhibits a shift towards higher diffraction angles as the annealing time increasing from 5 min to 30 min, which can be ascribed to the substitution of oxygen for nitrogen in TiN in the annealing process considering the fact that the atomic radius of oxygen is smaller than that of nitrogen [27]. Similar behavior has been reported and attributed to titanium oxynitride formation [28]. Further increasing the annealing time to 60 min and 120 min, the TiN (200) peaks disappear, indicating that the TiN may has been converted to TiO$_2$ which is observed by TEM as shown later.

Figure 2 displays the SEM images of samples with various annealing time. Top-view image in Figure 2(a) shows that the as-prepared TiN NRAs exhibit porous structure that consisted of nanorods with diameter of *ca*. 70~200 nm, and the gap between the nanorods is *ca*. 40~50 nm. The nanorods are found to be fairly uniform with length of *ca*. 600 nm,

which are separated by voids as shown clearly in the inset of Figure 2(a). Moreover, one can see that the nanorods are tilted with an angle of approximately 30° with respect to the substrate normal due to the high angle of the incident adatom plume to the substrate ($\alpha = 85°$) [24]. The porous structure was formed during the deposition process due to the self-shadowing effects and the limited mobility of the deposited atoms [29]. The morphologies of the TiN NRAs annealed at 330°C for 5 min, 15 min, 30 min, 60 min, and 120 min do not change and are identical with those of the as-deposited NRAs as shown in Figures 2(b)–2(f).

In order to further investigate the microstructures of the as-prepared TiN NRAs and the ones annealed, TEM is performed. Figure 3(a) shows the low-resolution TEM image of the as-prepared TiN NRAs. One can see that the nanorod is of length of *ca*. 600 nm and diameter of *ca*. 80 nm which
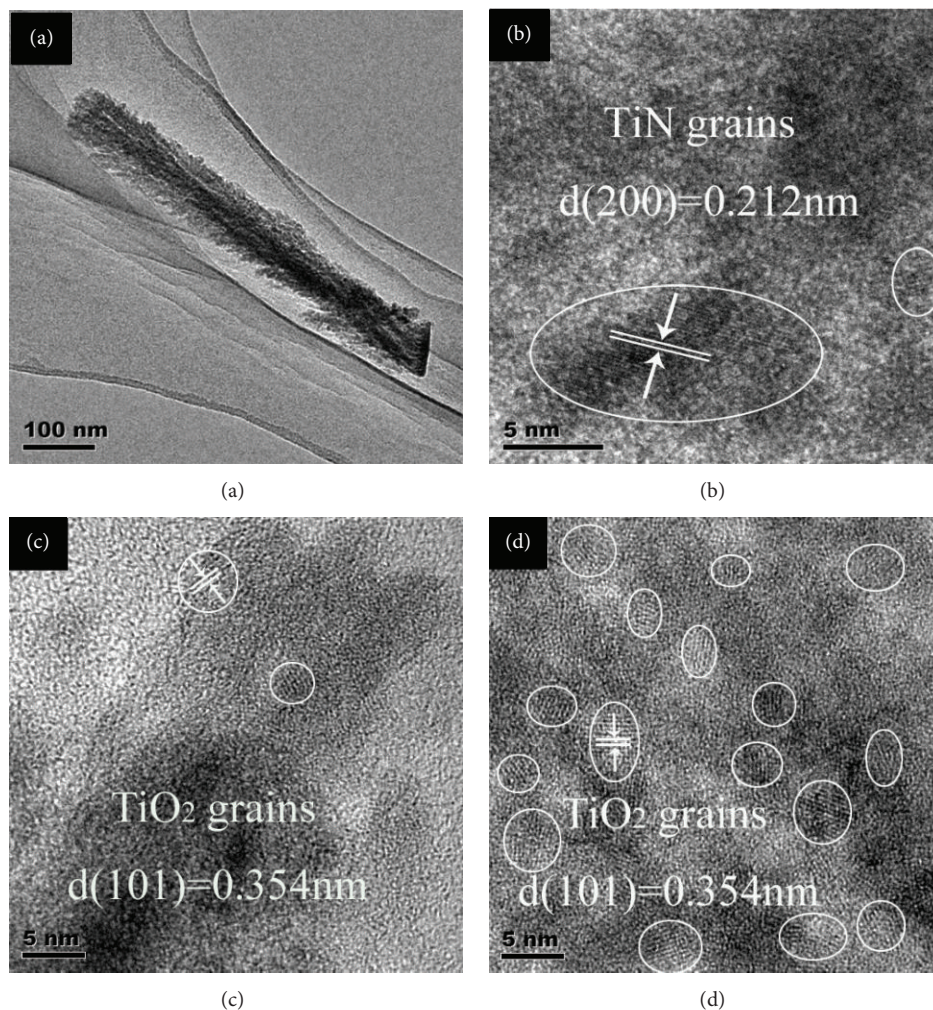
(a)

(b)

(c)

(d)

Figure 3: (a) Low-resolution TEM images of the as-prepared TiN NRAs; (b) high-resolution TEM (HRTEM) images of (a); (c) and (d) are the HR-TEM of the images of the 15 N-TiO$_2$ NRAs and 120 N-TiO$_2$, respectively.

is in agreement with the SEM results. The nanorod exhibits a pine needle structure, leading to a significant enhancement in the overall surface area, which is much higher than that of nanorod with smooth or uniform surface. This microstructure can facilitate the performance of photoelectrochemistry due to the 1D structure with high specific surface area. Figure 3(b) displays the high-resolution TEM (HRTEM) image of the as-prepared TiN NRAs. The TiN crystalline grains can be seen clearly with interplanar lattice spacing of 0.212 nm, corresponding well with that of (200) plane. TiN can be converted into TiO$_2$ by a complete oxidation in air at medium temperature [30, 31]. The oxidation occurs from the surface to the inner of nanorods with diffusion of O$_2$ through the gap between the nanorods [32]. The annealing time is the critical parameter in the oxidation process if the temperate is fixed. Large parts of TiO$_2$ are present in amorphous state in the 15 N-TiO$_2$ NRAs that were annealed for 15 min at 330°C, and only trace amount of TiO$_2$ crystalline grains with interplanar lattice spacing of 0.354 nm is formed as shown in Figure 3(c). Further increasing the annealing time to 120 min, there are a great number of TiO$_2$ crystalline grains and no

TiN crystalline is found as shown in Figure 3(d), which is in agreement with the XRD result.

Figure 4(a) shows the UV-visible light transmittance spectra of the TiN NRAs annealed for different times at 330°C. TiN films were assumed to be opaque with thickness of several tens of nanometers in previous report [32]; however, the transmittance of the as-prepared TiN NRAs in this study is *ca.* 25% in visible light. With increase in annealing time, the transmittance increases gradually at the wavelength of 300 nm to 600 nm, which may be due to the difference in the degree of oxidation of the films from TiN to TiO$_2$. The spectra are characterized by a good regularity of the interference fringes and a systematic increment in wavelength in which the film practically ceases to be transparent in the visible range. This behavior has been previously observed in TiO$_2$ doped with metals [33]. The optical gap (E_g) of the semiconductor with large band gap can be determined from the absorption coefficient α. If scattering effect is neglected, the absorption coefficient can be expressed by $(\alpha E_g)^n = A(Eg - \hbar v)$, where $n = 1/2$ for an indirect transmission [34]. It could be presumed that the film mixed
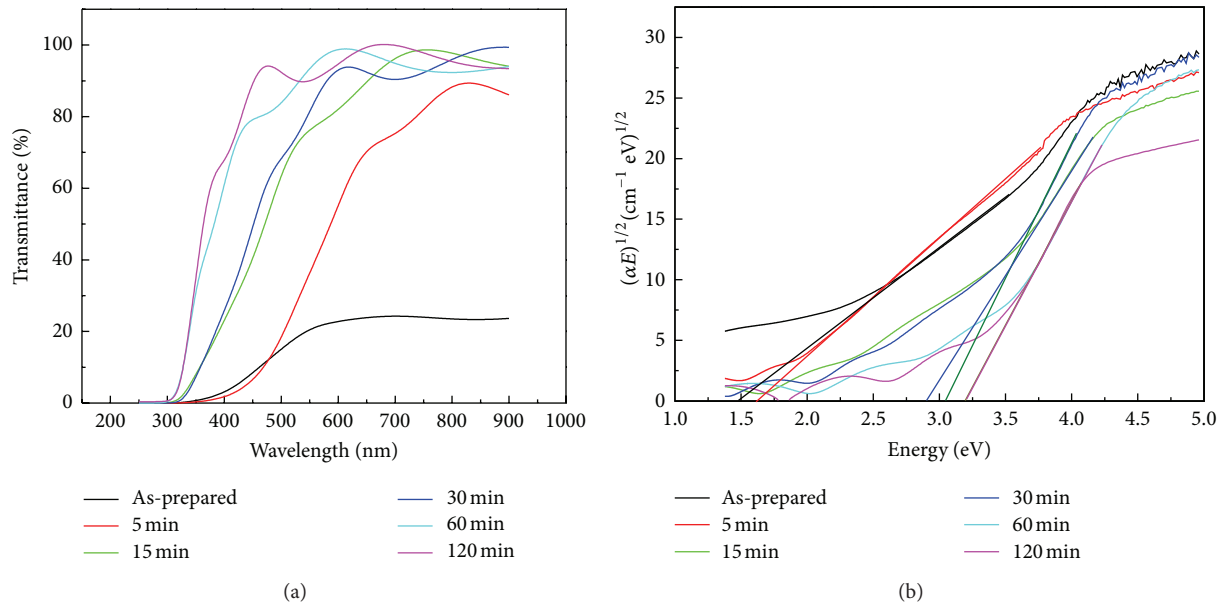
FIGURE 4: (a) Transmittance spectra of the N-doped TiO_2 NRAs annealed for different times at 330°C; (b) Tauc plot of $(\alpha E)^{1/2}$ versus photon energy ($E = h\nu$) for the N-doped TiO_2 NRAs annealed for different times at 330°C.

with TiO_2 and TiN is the indirect semiconductor [35], similar to TiO_2. The Tauc [36] plot of $(\alpha E)^{1/2}$ versus photon energy ($E = h\nu$) is shown in Figure 4(b). Usually, the band gap can be obtained by extrapolating the linear region to $(\alpha E)^{1/2} = 0$. The band gap of the as-deposited TiN NRAs is *ca.* 1.49 eV, corresponding well with the previous report [37]. The band gap of the 120 N-TiO_2 NRAs is 3.19 eV, which is very close to that of reported anatase TiO_2 (3.2 eV), showing that the TiN is converted to TiO_2 completely by annealing for 120 min [38]. The band gap varies from 1.49 eV to 3.19 eV with increase in annealing time. This result is particularly interesting from the photo-catalysis viewpoint because it is possible to tune the onset of the absorption to the desired visible wavelength.

Photocurrent intensity has been regarded as one of the most efficient methods to evaluate the photocatalytic activity of photocatalyst, and it has been recognized that a high photocurrent intensity suggests a high efficiency for electrons and holes generation and separation, and thus a high photo-catalytic activity [39]. To test the photoelectrochemical properties of the TiN NRAs annealed for different times at 330°C (i.e., N-doped TiO_2 NRAs) under visible light irradiation, photocurrent densities were measured in the light on-off process with a pulse of 30 s by the potentiostatic technique [40]. Under 130 mW/cm^2 of visible light illumination and 0 V bias versus Ag/AgCl, all of the N-doped TiO_2 NRAs exhibit photocurrents as shown in Figure 4(a). However, the photocurrent intensity of TiN NRAs can be neglected compared with that of the N-doped TiO_2 samples. For all N-doped TiO_2 NRAs, the photocurrent value goes down to zero as soon as the light is turned off, and the photocurrent intensity comes back to the original value as soon as the light is turned on again. Such a photocurrent response is highly reproducible for numerous on-off cycles.

For the N-doped NRAs, an initial fast increase in the photocurrent intensity is recorded, followed by a decrease in the photocurrent intensity with time under visible light; it can be assumed that lots of electrons and holes generated in the N-doped TiO_2 leading to a fast photocurrent intensity increase when the light is switched on, then electrons transfer through the nanorod and one part of the electrons vanishes in the recombination center, and the photocurrent intensity decreases and remains a steady state; this behavior is common for TiO_2 electrode and can be described in terms of a classical onset of recombination [41]. Among N-doped TiO_2 NRAs, the photocurrent intensity of which annealed for 15 min (15 N-TiO_2 NRAs) reaches a maximum, and the photocurrent intensity becomes lower while increasing or decreasing the annealing time, the phenomenon can be ascribed to the state and concentration of nitrogen in TiO_2 NRAs which will be discussed later. Figure 5(b) shows the *I-V* characteristics which confirm the superior performance of producing higher photocurrent intensities for the N-doped TiO_2 NRAs. The open circuit potential, V_{oc}, corresponds to the difference between the apparent Fermi level of the N-doped TiO_2 NRAs. The open circuit potential of 5 N-TiO_2 NRAs and 15 N-TiO_2 NRAs is *ca.* −0.055 V and −0.177 V, which is greater than that of bare TiN NRAs (V_{oc}: *ca.* 0.083 V), demonstrating a shift in the Fermi level to more negative potential as a result of N doping in TiO_2. As shown previously, better charge separation and electron accumulation in the semiconductor shift the Fermi level to more negative potential [42]. However, the V_{oc} of the 120 N-TiO_2 NRAs, which can be considered as pure TiO_2 that we discussed earlier, is 0.112 V, which is much positive than that of TiN NRAs. That the V_{oc} varies may be attributed to the difference in concentration and the state of N in TiO_2. Figure 5(c) shows a relationship between the band gap, photocurrent intensity,
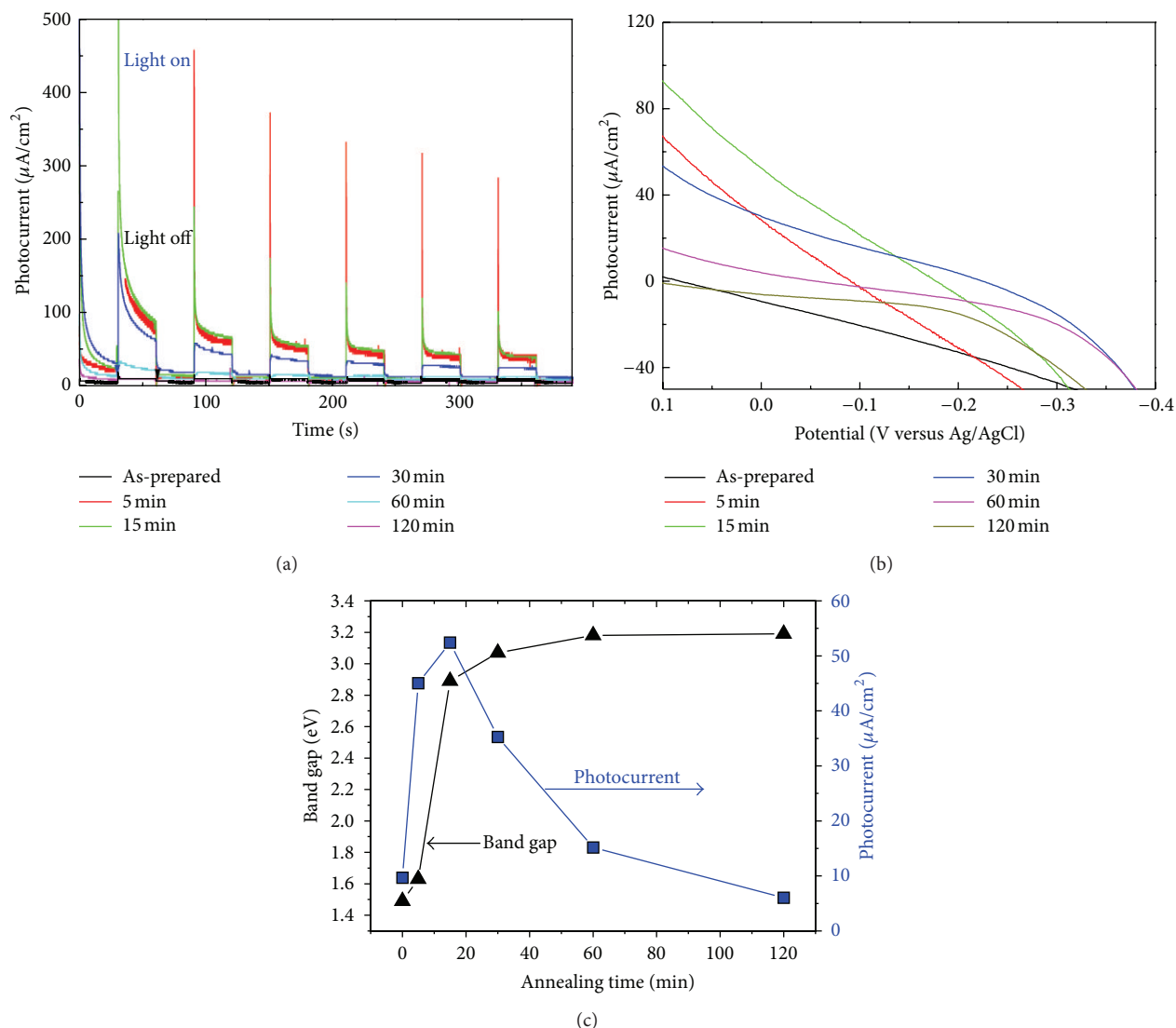
(a)

(b)

(c)

FIGURE 5: (a) Current versus time measurements of the N-doped TiO_2 NRAs annealed for different times at 330°C under 0 V bias versus Ag/AgCl; (b) *I-V* characteristics of the N-doped TiO_2 NRAs annealed for different times at 330°C; (c) relationship of the band gap, photocurrent intensity, and annealing time.

and annealing time. With the annealing time decreasing, the photocurrent intensity increases from *ca.* 6.04 μA/cm^2 (120 N-TiO_2 NRAs) to 52.43 μA/cm^2 (15 N-TiO_2 NRAs), which can be ascribed to the narrower band gap from 3.19 eV to 2.89 eV. However, the photocurrent intensity of 5 N-TiO_2 NRAs decreases as compared with that of 15 N-TiO_2 NRAs. Therefore, the optimal condition for obtaining photocurrent intensity is controlling the annealing time in the range from 5 min to 15 min in this system.

Figure 6 shows the N 1*s* XPS spectra core level of as-prepared TiN and which was obtained from the TiN NRAs annealed for 5 min, 15 min, and 120 min. For the as-prepared TiN, there is a peak at ~395.9 eV, which is characteristic of N^{3-} corresponding to TiN, [13, 43] and the N 1*s* peak at ~398.8 eV can be ascribed to chemisorbed molecular nitrogen [44]. The N 1*s* peak at ~399.6 eV in 5 N-TiO_2 and 15 N-TiO_2 is ascribed to the incorporated nitrogen dopant in

TiO_2 as interstitial N with formation of Ti-N-O or Ti-O-N oxynitride [43, 45]. It is supported that the peak at 400.3 eV for 120 N-TiO_2 NRAs can be assigned to well-screened γ-N (essentially adsorbed N) [13] and the high binding energy peaks (401.6 eV and 402.7 eV) are generally considered to be characteristic of N–O bonds [46], while the peaks at 398.5 eV can also be ascribed to chemisorbed molecular nitrogen. In the oxidation process, TiN is converted to TiO_2 gradually as shown in previous results, and the nitrogen is substituted by oxygen due to the higher active of oxygen, forming Ti-N-O bond as shown in the 5 N-TiO_2 NRAs and 15 N-TiO_2 NRAs. At the same time, the peak at 395.9 eV ascribed to TiN vanishes in 120 N-TiO_2 NRAs, which is in agreement with the TEM results (Figure 3(d)). It can be assumed that the photoelectrochemical performance of the N-doped TiO_2 in visible light is attributed to the result of mixing of N 2p acceptor states located just above the top of the valence band
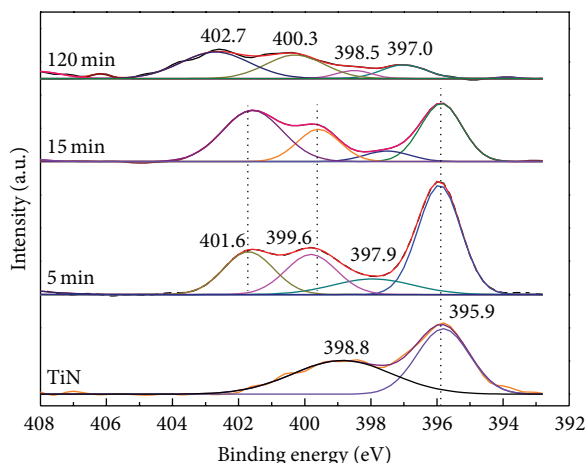
FIGURE 6: XPS spectra of the N 1s core level obtained from the as-prepared TiN, 5 N-TiO$_2$ NRAs, 15 N-TiO$_2$ NRAs, and 120 N-TiO$_2$ NRAs, respectively.

with the O 2p states of TiO$_2$, which empower them with visible-light driven photocatalytic ability [9]. The photocurrent intensity is 6.04 μA/cm^2, 52.43 μA/cm^2, 45.02 μA/cm^2 for the 120 N-TiO$_2$ NRAs, 15 N-TiO$_2$ NRAs, and 5 N-TiO$_2$ NRAs, respectively, and the photocurrent intensity of 15 N-TiO$_2$ NRAs reaches the maximum. However, the integrated area for the peak at 399.6 eV, which is considered as the concentration of doping N in TiO$_2$, is 0%, 17.29%, and 18.68%, respectively. It may indicate that N dopant enhances the photocurrent intensity, but exceeding content of N will decrease the photocurrent density because of the generation of electron-hole recombination centers arising from higher doping impurities [17]. Therefore, it is very important to control the doped nitrogen concentration in TiO$_2$ to obtain a high photocurrent intensity in visible light.

4. Summary

In summary, N-doped TiO$_2$ NRAs were prepared by annealing the TiN NRAs which were deposited by means of angle deposition (OAD) technique. The TiN NRAs were annealed at 330°C for different times (5 min, 15 min, 30 min, 60 min, and 120 min). The band gap of annealed TiN NRAs (N-doped TiO$_2$ NRAs) shows a significant variance with annealing time and can be controlled readily by varying annealing time. All of N-doped TiO$_2$ NRAs exhibit enhanced photocurrent intensity when irradiated in visible light, and the one annealed for 15 min has the maximum photocurrent intensity owing to the optimal N dopant concentration. The results are very promising for the band gap modification with the application in photocatalysis.

Acknowledgments

References

[1] A. Fujishima and K. Honda, "Electrochemical photolysis of water at a semiconductor electrode," *Nature*, vol. 238, no. 5358, pp. 37–38, 1972.

[2] R. Yuan, T. Chen, E. Fei et al., "Surface chlorination of TiO$_2$-based photocatalysts: a way to remarkably improve photocatalytic activity in both UV and visible region," *ACS Catalysis*, vol. 1, no. 3, pp. 200–206, 2011.

[3] E. Barborini, A. M. Conti, I. Kholmanov et al., "Nanostructured TiO$_2$ films with 2 eV optical gaps," *Advanced Materials*, vol. 17, no. 15, pp. 1842–1846, 2005.

[4] R. Abe, "Recent progress on photocatalytic and photoelectrochemical water splitting under visible light irradiation," *Journal of Photochemistry and Photobiology C*, vol. 11, no. 4, pp. 179–209, 2010.

[5] Y. Park, S.-H. Lee, S. O. Kang, and W. Choi, "Organic dye-sensitized TiO$_2$ for the redox conversion of water pollutants under visible light," *Chemical Communications*, vol. 46, no. 14, pp. 2477–2479, 2010.

[6] B. Liu, D. Wang, Y. Zhang et al., "Photoelectrical properties of Ag$_2$S quantum dot-modified TiO$_2$ nanorod arrays and their application for photovoltaic devices," *Dalton Transactions*, vol. 42, no. 6, pp. 2232–2237, 2013.

[7] S. Liu, E. Guo, and L. Yin, "Tailored visible-light driven anatase TiO$_2$ photocatalysts based on controllable metal ion doping and ordered mesoporous structure," *Journal of Materials Chemistry*, vol. 22, no. 11, pp. 5031–5041, 2012.

[8] S. G. Kumar and L. G. Devi, "Review on modified TiO$_2$ photocatalysis under UV/visible light: selected results and related mechanisms on interfacial charge carrier transfer dynamics," *Journal of Physical Chemistry A*, vol. 115, no. 46, pp. 13211–13241, 2011.

[9] R. Asahi, T. Morikawa, T. Ohwaki, K. Aoki, and Y. Taga, "Visible-light photocatalysis in nitrogen-doped titanium oxides," *Science*, vol. 293, no. 5528, pp. 269–271, 2001.

[10] T. Ohno, M. Akiyoshi, T. Umebayashi, K. Asai, T. Mitsui, and M. Matsumura, "Preparation of S-doped TiO$_2$ photocatalysts and their photocatalytic activities under visible light," *Applied Catalysis A*, vol. 265, no. 1, pp. 115–121, 2004.

[11] W. Ho, J. C. Yu, and S. Lee, "Synthesis of hierarchical nanoporous F-doped TiO$_2$ spheres with visible light photocatalytic activity," *Chemical Communications*, no. 10, pp. 1115–1117, 2006.

[12] Y. Choi, T. Umebayashi, and M. Yoshikawa, "Fabrication and characterization of C-doped anatase TiO$_2$ photocatalysts," *Journal of Materials Science*, vol. 39, no. 5, pp. 1837–1839, 2004.

[13] A. Ghicov, J. M. Macak, H. Tsuchiya et al., "Ion implantation and annealing for an efficient N-doping of TiO$_2$ nanotubes," *Nano Letters*, vol. 6, no. 5, pp. 1080–1082, 2006.

[14] D. N. Tafen, J. Wang, N. Wu, and J. P. Lewis, "Visible light photocatalytic activity in nitrogen-doped TiO$_2$ nanobelts," *Applied Physics Letters*, vol. 94, no. 9, Article ID 093103, pp. 093101–093101, 2009.

[15] F. Peng, L. Cai, L. Huang, H. Yu, and H. Wang, "Preparation of nitrogen-doped titanium dioxide with visible-light photocatalytic activity using a facile hydrothermal method," *Journal of Physics and Chemistry of Solids*, vol. 69, no. 7, pp. 1657–1664, 2008.

[16] G. Liu, H. G. Yang, X. Wang et al., "Visible light responsive nitrogen doped anatase TiO_2 sheets with dominant {001} facets derived from TiN," *Journal of the American Chemical Society*, vol. 131, no. 36, pp. 12868–12869, 2009.

[17] L. Zhu, J. Xie, X. Cui, J. Shen, X. Yang, and Z. Zhang, "Photoelectrochemical and optical properties of N-doped TiO_2 thin films prepared by oxidation of sputtered TiN_x films," *Vacuum*, vol. 84, no. 6, pp. 797–802, 2010.

[18] U. Shaislamov and B. L. Yang, "CdS-sensitized single-crystalline TiO_2 nanorods and polycrystalline nanotubes for solar hydrogen generation," *Journal of Materials Research*, vol. 1, no. 1, pp. 1–6, 2013.

[19] H. Zhou, Y. Qu, T. Zeid, and X. Duan, "Towards highly efficient photocatalysts using semiconductor nanoarchitectures," *Energy & Environmental Science*, vol. 5, no. 5, pp. 6732–6743, 2012.

[20] S. K. Pradhan, P. J. Reucroft, F. Yang, and A. Dozier, "Growth of TiO_2 nanorods by metalorganic chemical vapor deposition," *Journal of Crystal Growth*, vol. 256, no. 1, pp. 83–88, 2003.

[21] J.-N. Nian and H. Teng, "Hydrothermal synthesis of single-crystalline anatase TiO_2 nanorods with nanotubes as the precursor," *The Journal of Physical Chemistry B*, vol. 110, no. 9, pp. 4193–4198, 2006.

[22] L. González-García, I. González-Valls, M. Lira-Cantu, A. Barranco, and A. R. González-Elipe, "Aligned TiO_2 nanocolumnar layers prepared by PVD-GLAD for transparent dye sensitized solar cells," *Energy & Environmental Science*, vol. 4, no. 9, pp. 3426–3435, 2011.

[23] Y. He, Z. Zhang, and Y. Zhao, "Optical and photocatalytic properties of oblique angle deposited TiO_2 nanorod array," *Journal of Vacuum Science & Technology B*, vol. 26, no. 4, pp. 1350–1358, 2008.

[24] A. Wolcott, W. A. Smith, T. R. Kuykendall, Y. Zhao, and J. Z. Zhang, "Photoelectrochemical water splitting using dense and aligned TiO_2 nanorod arrays," *Small*, vol. 5, no. 1, pp. 104–111, 2009.

[25] K. M. Krause, M. T. Taschuk, K. D. Harris et al., "Surface area characterization of obliquely deposited metal oxide nanostructured thin films," *Langmuir*, vol. 26, no. 6, pp. 4368–4376, 2009.

[26] X. Zhang, Q. Zhou, J. Ni, Z. Li, and Z. Zhang, "Surface-enhanced Raman scattering from a hexagonal lattice of micro-patterns of vertically aligned Ag nanorods," *Physica E*, vol. 44, no. 2, pp. 460–463, 2011.

[27] R. Shannon, "Revised effective ionic radii and systematic studies of interatomic distances in halides and chalcogenides," *Acta Crystallographica A*, vol. 32, no. 5, pp. 751–767, 1976.

[28] J. Guillot, A. Jouaiti, L. Imhoff et al., "Nitrogen plasma pressure influence on the composition of TiN_xO_y sputtered films," *Surface and Interface Analysis*, vol. 33, no. 7, pp. 577–582, 2002.

[29] M. Suzuki, "Practical applications of thin films nanostructured by shadowing growth," *Journal of Nanophotonics*, vol. 7, no. 1, pp. 073598–073598, 2013.

[30] J. Desmaison, P. Lefort, and M. Billy, "Oxidation mechanism of titanium nitride in oxygen," *Oxidation of Metals*, vol. 13, no. 6, pp. 505–517, 1979.

[31] H. G. Tompkins, "Oxidation of titanium nitride in room air and in dry O_2," *Journal of Applied Physics*, vol. 70, no. 7, pp. 3876–3880, 1991.

[32] H. Van Bui, A. Groenland, A. Aarnink, R. Wolters, J. Schmitz, and A. Kovalgin, "Growth kinetics and oxidation mechanism of ALD TiN thin films monitored by in situ spectroscopic ellipsometry," *Journal of the Electrochemical Society*, vol. 158, no. 3, pp. H214–H220, 2011.

[33] A. L. J. Pereira, L. Gracia, A. Beltrán, P. N. Lisboa-Filho, J. H. D. da Silva, and J. Andrés, "Structural and electronic effects of incorporating Mn in TiO_2 films grown by sputtering: anatase versus rutile," *Journal of Physical Chemistry C*, vol. 116, no. 15, pp. 8753–8762, 2012.

[34] N. Miyata and S. Akiyoshi, "Preparation and electrochromic properties of rf-sputtered molybdenum oxide films," *Journal of Applied Physics*, vol. 58, no. 4, pp. 1651–1655, 1985.

[35] W. Smith, H. Fakhouri, J. Pulpytel, and F. Arefi-Khonsari, "Control of the optical and crystalline properties of TiO_2 in visible-light active TiO_2/TiN bi-layer thin-film stacks," *Journal of Applied Physics*, vol. 111, no. 2, 2012.

[36] J. Tauc, *Optical Properties of Solids*, North-Holland, Amsterdam, The Netherlands, 1972.

[37] J. Huang and C. Xu, "Effect of N_2 mass flow rate on the optical property of titanium nitride films deposited by magnetron sputtering," *Acta Optica Sinica*, vol. 25, no. 9, pp. 1293–1296, 2005.

[38] K. G. Grigorov, I. C. Oliveira, H. S. Maciel et al., "Optical and morphological properties of N-doped TiO_2 thin films," *Surface Science*, vol. 605, no. 7-8, pp. 775–782, 2011.

[39] Y. Liu, C. Xie, J. Li, T. Zou, and D. Zeng, "New insights into the relationship between photocatalytic activity and photocurrent of TiO_2/WO_3 nanocomposite," *Applied Catalysis A*, vol. 433-434, pp. 81–87, 2012.

[40] G. Li, L. Wu, F. Li, P. Xu, D. Zhang, and H. Li, "Photoelectrocatalytic degradation of organic pollutants via a CdS quantum dots enhanced TiO_2 nanotube array electrode under visible light irradiation," *Nanoscale*, vol. 5, no. 5, pp. 2118–2125, 2013.

[41] X. Cui, M. Ma, W. Zhang, Y. Yang, and Z. Zhang, "Nitrogen-doped TiO_2 from TiN and its visible light photoelectrochemical properties," *Electrochemistry Communications*, vol. 10, no. 3, pp. 367–371, 2008.

[42] M. Jakob, H. Levanon, and P. V. Kamat, "Charge distribution between UV-irradiated TiO_2 and gold nanoparticles: determination of shift in the Fermi level," *Nano Letters*, vol. 3, no. 3, pp. 353–358, 2003.

[43] J. Wang, D. N. Tafen, J. P. Lewis et al., "Origin of photocatalytic activity of Nitrogen-doped TiO_2 nanobelts," *Journal of the American Chemical Society*, vol. 131, no. 34, pp. 12290–12297, 2009.

[44] A. Trenczek-Zajac, M. Radecka, K. Zakrzewska et al., "Structural and electrical properties of magnetron sputtered Ti(ON) thin films: the case of TiN doped *in situ* with oxygen," *Journal of Power Sources*, vol. 194, no. 1, pp. 93–103, 2009.

[45] R. Jansen and H. van Bekkum, "XPS of nitrogen-containing functional groups on activated carbon," *Carbon*, vol. 33, no. 8, pp. 1021–1027, 1995.

[46] X. Chen, Y. B. Lou, A. C. Samia, C. Burda, and J. L. Gole, "Formation of oxynitride as the photocatalytic enhancing site in nitrogen-doped titania nanocatalysts: comparison to a commercial nanopowder," *Advanced Functional Materials*, vol. 15, no. 1, pp. 41–49, 2005.